Sādhanā (2020) 45:287
https://doi.org/10.1007/s12046-020-01520-0

An image processing method to measure droplet impact and evaporation on a solid surface

AMITOSH DASH[1], PRATHAMESH G BANGE[1], NAGESH D PATIL[2] and RAJNEESH BHARDWAJ[1,*]

[1]Department of Mechanical Engineering, Indian Institute of Technology Bombay, Mumbai 400076, India
[2]Department of Mechanical Engineering, Indian Institute of Technology Bhilai, Raipur 492015, India
e-mail: rajneesh.bhardwaj@iitb.ac.in

MS received 19 April 2020; revised 14 September 2020; accepted 6 October 2020

Abstract. We employ high-speed visualization to quantify the impact and evaporation of a droplet on a solid surface. The time-varying droplet shapes are recorded using a high-speed camera and an image processing method is developed for measurement for droplet dimensions, dynamic contact angle, and volume. The method is based on the liquid-gas and liquid-solid interface detection using Canny's method and Otsu's method for threshold digitalization. To obtain the dynamic contact angle, a higher-order polynomial is fitted along the pixels near the contact line. The droplet volume is measured assuming an axisymmetric geometry of the droplet and numerically integrating the identified pixels in the droplet. We demonstrate the detection of the complex topology of the deforming liquid-gas interface of an impacting and evaporating droplet on a solid surface. We plot the time-variation of droplet dimensions, namely, wetted diameter, maximum diameter, height; dynamic contact angle, and droplet volume. The contact angle and volume measurements are verified with known analytical values. Three case studies are considered to demonstrate the capability of the proposed method, namely, sessile evaporating droplet, bouncing droplet, and spreading viscous droplet on a solid surface.

Keywords. Droplet impact; droplet evaporation; image processing method; contact angle.

1. Introduction

Droplet impact and evaporation are useful for several technical applications such as ink-jet printing, spray coating, and surface cooling via spray evaporative cooling [1] and pool boiling [2]. Recently, the mechanisms of the formation of dried deposits of colloidal particles by an evaporating sessile droplet has been a much-studied problem (for example, see review of such studies in [3, 4]). The impact and evaporation process is highly transient [5, 6] and high-speed visualization is one of the key techniques to record time-varying droplet shapes (see a review of visualization techniques in [7]). Experimental protocols for recording the sample preparations and recording images of advancing and receding contact angles of a water droplet on a solid surface were recently reported by Huhtamäki *et al* [8]. The accurate determination of the droplet dimensions, volume, and dynamic contact angle from the visualization images are important to reduce measurement errors.

Previous studies on the contact angle measurement mostly focused on static droplets with a non-moving contact line, as reviewed recently by Chini and Amirfazli [9]. These methods are classified as tensiometry and goniometry methods [9]. The former applies the Young equation at the contact line to estimate contact angle in terms of surface energies and hence its accuracy depends on these surface energies. The latter is based on the image processing method and requires two-dimensional side image of the droplet for the contact angle measurement. Several previous reports in this category utilize a technique called axisymmetric drop shape analysis [10–14] developed by Neumann and co-workers. In this technique, the recorded axisymmetric droplet profile is fitted with the Young-Laplace equation using numerical integration, with the minimum error between the former and latter. The contact angle is measured as the slope of the fitted curve at the contact line. Similarly, Bateni *et al* [15] used higher-order polynomial fitting at the contact line to obtain the contact angle. Stalder *et al* [16] proposed a 'Dropsnake method' in which the B-spline curve was fitted to the droplet profile, which requires very few points on the droplet boundary for the fitting. Recently, Chini and Amirfazli [9] presented a sub-pixel polynomial fitting based method in which the contact line is accurately found by fitting a sigmoid function [14] for pixel intensity across the liquid-gas interface. In the context of

*For correspondence
Published online: 19 November 2020

droplet volume measurement, Thurow *et al* [17] proposed an image processing method to measure the droplet volume based on the numerical integration of pixel slices in the vertical direction for a spherical droplet.

Most of the previously reported image processing based methods for measuring contact angle were for static, axisymmetric droplets and did not consider the impact dynamics. The droplet dimensions were mostly measured by manual pixel counting from an imaging software, which may induce an error on the order of pixel size or imaging resolution [5–7]. Thus, low-resolution images are more susceptible to larger measurement errors. While previous studies have measured the time-varying droplet volume by monitoring the mass of the droplet, for instance, by a nanomechanical resonator [18], the present method uses planar images which is cheaper, robust, and accurate with reasonable fidelity. A previous study by Thurow *et al* [17] reported the volume measurement of an airborne dispensed droplet by using an imaging technique, however, the present approach is more versatile and robust than that in [17], since we integrate each pixel instead of a pixel slice in the vertical direction. Besides, the previous methods did not report the volume measurement of an impacting or deforming droplet, to the best of our knowledge.

The objective of the present paper is to propose an accurate and versatile image processing method for quantifying droplet impact and evaporation on a solid surface. We employ the Canny method with the Otsu threshold to detect the liquid-gas and liquid-solid interface. To measure the contact angle, we use the sub-pixel polynomial fitting method, as proposed by Chini and Amirfazli [9]. The time-varying droplet dimensions, namely, wetted diameter, maximum diameter, height are measured using the sub-pixel location, to reduce the measurement errors, especially for low imaging resolution. The droplet volume is measured assuming the axisymmetric geometry of the droplet and numerically integrating the identified pixels in the droplet.

The remainder of the paper is organized as follows. The image processing method is described in section 2 to measure the time-varying parameters to quantity the droplet dynamics. We test the method for three case studies - sessile evaporating droplet (section 3.1), bouncing droplet (section 3.2), and spreading viscous droplet (section 3.3) - to demonstrate the capability of the present method to capture the large time-variation of wetted diameter, height, contact angle, and volume.

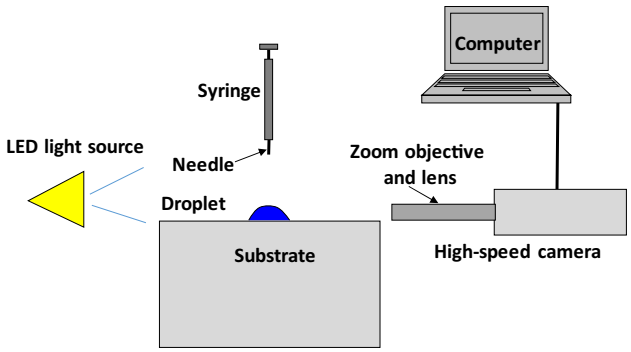

Figure 1. Schematic of the experimental set-up used in the present study.

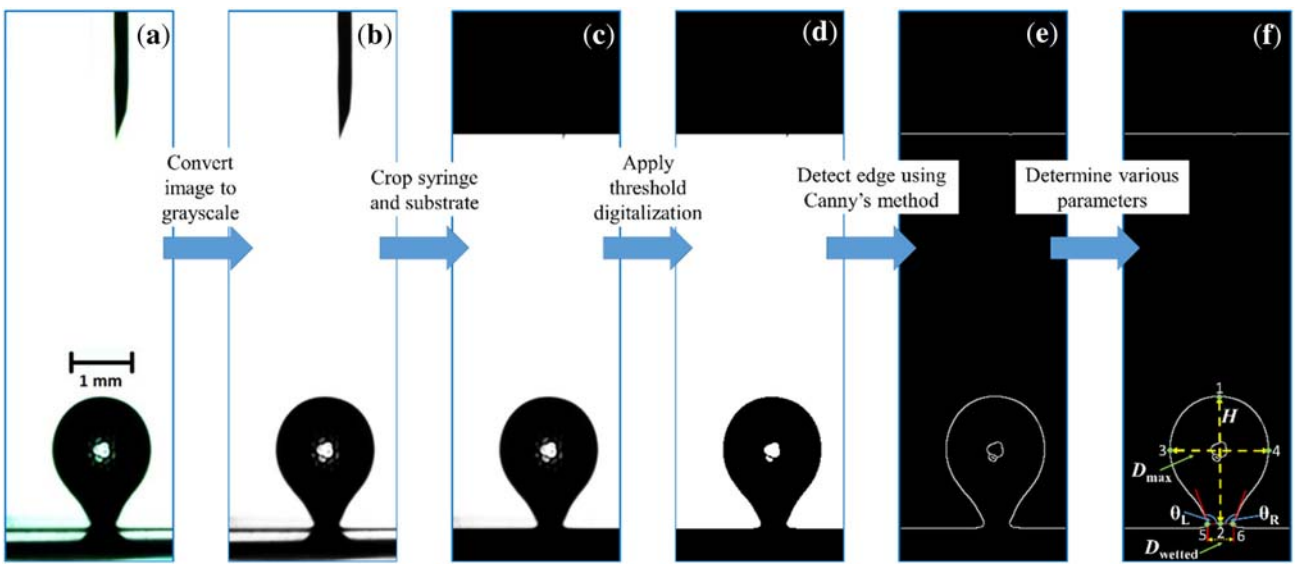

Figure 2. (a) Original color image, (b) Converted image to grayscale, (c) Image obtained after cropping syringe and substrate, (d) Image obtained after applying threshold digitalization, (e) Liquid-gas and liquid-solid interface detection using Canny's method, (f) Definition of various droplet parameters.

2. Methods

Microliter water and glycerol droplets are generated using a syringe attached with 31 gauge needle which has 133 ± 19 μm inner diameter. The diameter of the water and glycerol droplets are 1.7 ± 0.05 and 1.6 ± 0.05 mm, respectively. The height of the syringe from the substrate surface is adjusted to obtain the desired impact velocity just before the impact. The impact and evaporation of the water droplet are studied on micropillared hydrophobic surface while the spreading of the glycerol droplet is recorded on a silicon wafer. The micropillared surface is fabricated using standard photolithography techniques and briefly described in our previous work [19]. The width and height of square pillars are 20±2 μm and 27±1 μm, respectively. A surface with a pitch of 42 μm is used in the present study. The scanning electronic microscopy (SEM) image of the surface can be found in [19]. The equilibrium contact angle of the water droplet on the micropillared surface is around 145±3°. The impacting and evaporating droplets were visualized from the side using a high-speed camera (MotionPro, Y-3 classic, CMOS, C-mount) with long-distance working objective (Qioptiq Inc.), as shown schematically in figure 1. A white LED is used as a backlight source and an imaging resolution of 14 μm per pixel is obtained for all cases described in the present study. The pixel aspect ratio (PAR) is 1:1. The obtained videos are processed to get the color images using open-source software VirtualDub® [20]. The different components of the proposed image processing method are described in the following subsections. We use Matlab® 2014 [21] for the implementation of the proposed method.

2.1 *Liquid-gas and solid-gas interface detection*

We employ Canny's method [22] to detect liquid-gas and liquid-solid interface. In this method, the interface is tracked using local maxima of the gradient of the pixel intensity. This method uses two threshold values of the gradient to detect strong and weak interfaces and is more likely to detect true weak interfaces [22, 23]. The threshold values are calculated using Otsu's method [24, 25], a similar approach utilized by Chini and Amirfazli [9]. Note that the Otsu's method chooses the threshold to minimize the intra-class variance of the black and white pixels [24, 25]. As illustrated in figure 2, the process involved in detecting the interface is as follows:

- Convert the colored image into grayscale (figure 2b).
- Crop out the syringe and substrate (figure 2c).
- Digitalize the image using the threshold value determined by Otsu's method [24, 25] (figure 2d).
- Apply Canny's method [22, 23] to obtain the liquid-gas and liquid-solid interface (figure 2e). Note that in some cases the detected interface is discontinuous, hence we digitalize the image before using Canny's method.

2.2 *Droplet dimensions measurement*

Droplet dimensions are quantified in terms of wetted diameter (D_{wetted}), maximum diameter (D_{max}), and droplet height (H), as defined in the inset of figure 2f. The extremities of the liquid-gas interface (topmost, leftmost, rightmost) and location of the contact line were determined using the subpixel location by fitting a sigmoid function for pixel intensity, as described by Kalantrian *et al* [14] and later used by Chini and Amirfazli [9]. We fit the sigmoid function to a gray level profile perpendicular to the drop

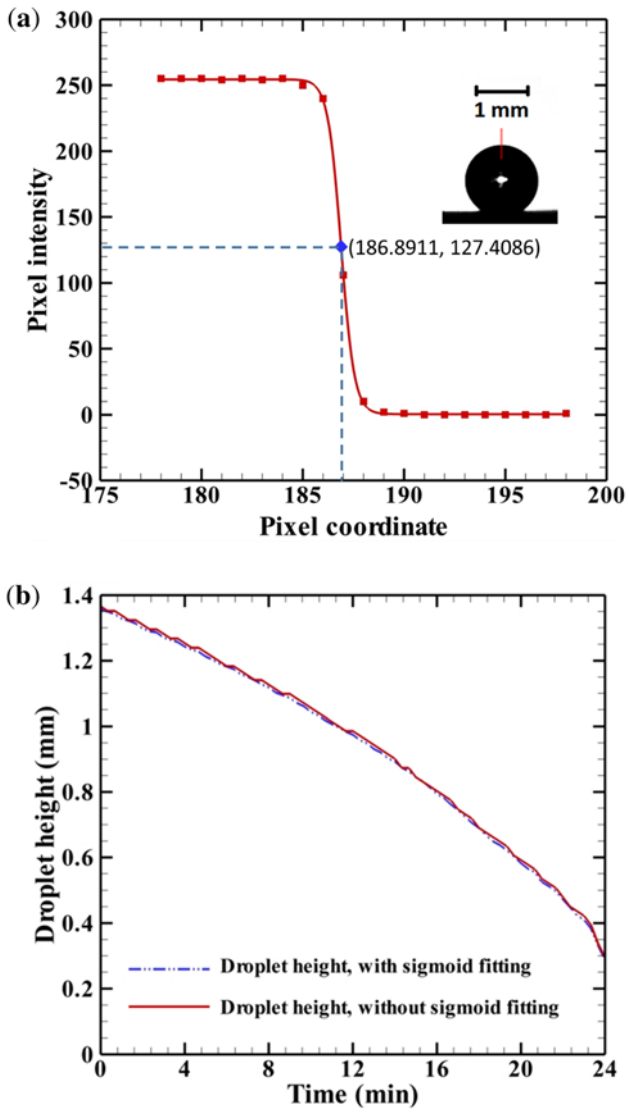

Figure 3. (a) Fitting of a sigmoid function across liquid-gas interface around the apex of the droplet, as shown in the inset along a red line, (b) Comparison between the droplet height obtained with and without sigmoid function.

interface at the topmost point. For instance, a sigmoid profile is fitted through the pixel intensities along the dotted line, shown in the inset of figure 3a and the actual edge is determined as the point with the maximum gradient in pixel intensity, shown as a dot on the fitted profile in figure 3a. We consider an example of the determination of the droplet height of an evaporating droplet and compare the time-variation of height determined using with and without sigmoid fitting in figure 3b, the one with sigmoid fitting is smoother and kink-free.

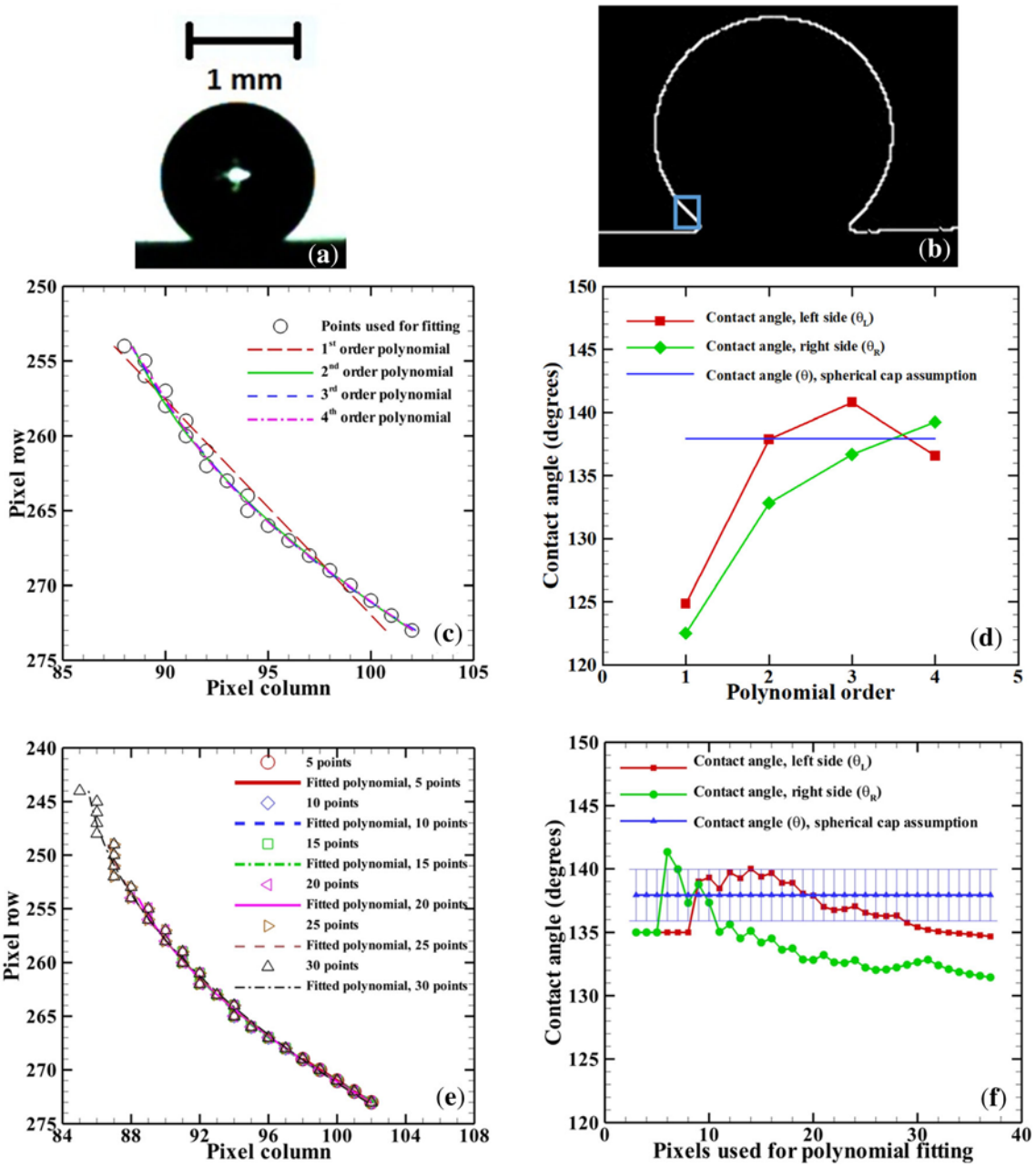

Figure 4. (a) Image of an evaporating sessile droplet considered for evaluating fidelity of the contact angle measurement, (b) Detected liquid-gas interface with a box, representing the region to measure contact angle, (c) Comparison of fitting of the polynomial of different orders on the points near the contact line, (d) Effect of order of the polynomial used for fitting on measured contact angle. Assuming droplet shape as a spherical cap, the theoretical contact angle is also plotted, (e) Second-order polynomial fitting with a different number of points used in the fitting, (f) Effect of the number of pixels used for fitting for the measured contact angle. Assuming droplet shape as a spherical cap, the theoretical contact angle is plotted with an error bar.

2.3 *Dynamic contact angle measurement*

After identifying the location of the contact line as described in section 2.1, we fit a polynomial to the pixel locations near the contact line to determine the contact angle and the contact angle is equal to the slope of the fitted polynomial at the contact line. To find the order of fitted polynomial and the number of pixels needed for the fitting, we consider a sessile droplet on a solid surface, shown in figure 4a. The blue box in figure 4b demarcates the liquid-gas interface selected for polynomial fitting. The polynomials of different orders are fitted along 20 pixel locations shown by hollow circles in figure 4c. The second, third, and fourth-order polynomial converge to describing the liquid-gas interface.

In this case, since gravity is negligible and surface forces dominate, the droplet profile is a spherical cap, with theoretical contact angle, $\tan(\theta/2) = h/r$, where h and r are the droplet height and wetted radius, respectively. We use this theoretical value to compare the results for polynomials of the different orders. As noted in figure 4d, the measured contact angle converge to the theoretical value for order $\geq$ 2, and the maximum error using the second-order polynomial is around 0% and 2% for the left and right measured contact angle, respectively. Thus the second-order polynomial is deemed adequate for measuring the contact line. In figure 4e and figure 4f, we study the effect of the number of pixels used for fitting on the measured contact angle with a second-order polynomial. We vary the number of pixels from 5 to 30 with a step of 5 and the fitted second-order polynomials are plotted in figure 4e. The number of pixels in the droplet height is around 87 in this case. The measured contact angles with different pixels are plotted in figure 4f and we observe minimum error ($\sim$3%) with around 15 pixels. The pixels 0 and 40 in figure 4f corresponds to 0 μm and 560 μm, respectively.

2.4 *Droplet volume measurement*

The droplet volume is calculated by numerically integrating the pixels in the droplet, assuming an axisymmetric impact and evaporation. The steps involved are as follows:

- Use the liquid-gas interface obtained in section 2.1 and extract the object with the longest perimeter in this image [26]. The reflection of the light coming from the illumination source is visible at the center of the droplet as a white spot and it is removed after the extraction, as shown in figure 5b. If the droplet is in contact with the substrate, the combined length of the liquid-gas and the liquid-solid interface is expected to be the object with the longest perimeter, as shown in figure 5b. If the droplet is not in contact with the substrate, we eliminate the substrate before filtering to make the liquid-gas interface as the object with the longest perimeter.
- Enclose the longest perimeter thus obtained in the above step, by adding pixels with white intensity to the substrate boundary, as illustrated in figure 5c. Note that if the droplet is not touching the surface, the droplet shape automatically creates the enclosed perimeter and this step is not needed.

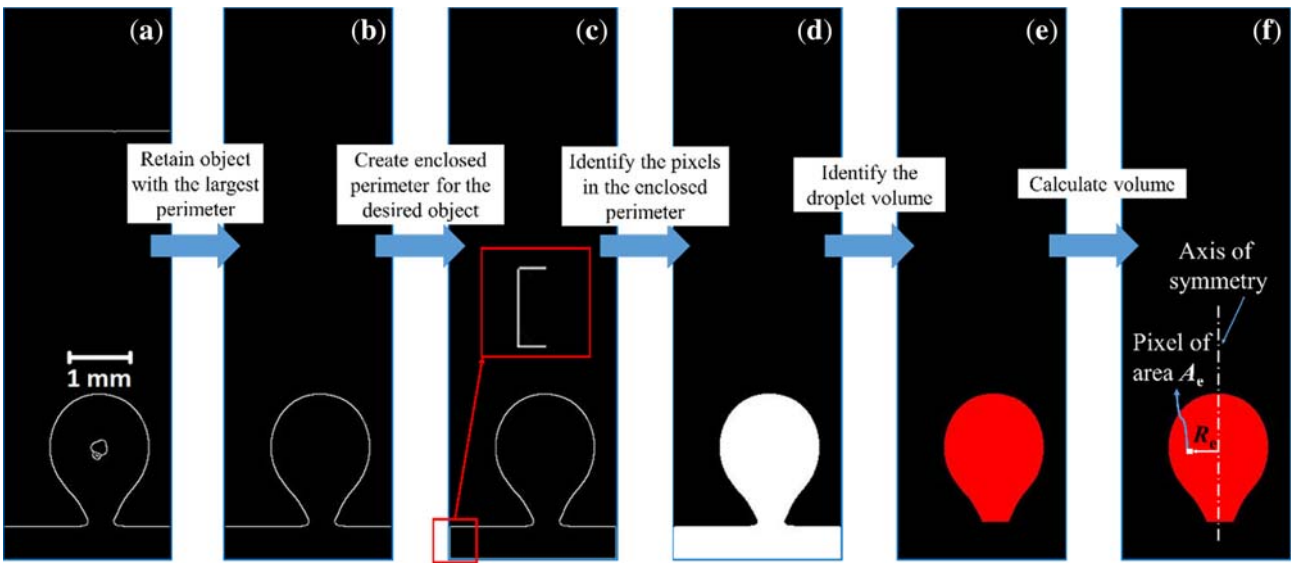

Figure 5. (a) Detected liquid-gas and liquid-solid interface, (b) Retaining the object with the largest perimeter, (c) Creating an enclosed region to identify the droplet, (d) Filling the previously created void, (e) Identifying the droplet volume, (f) Droplet volume representation assuming axisymmetric geometry.

- Utilize an algorithm based on morphological reconstruction [27, 28] to identify a set of pixels in the enclosed perimeter obtained in the previous step (figure 5d).
- Crop the substrate off from the set of pixels obtained in the previous step to obtain the pixels inside the droplet. (Figure 5e).
- Considering axisymmetric geometry as shown in figure 5f, the droplet volume is $V = \frac{1}{2}\sum_{i=1}^{n} 2\pi R_e A_e$ where n is the number of pixels contained in the droplet volume, A_e is the area of a pixel at radial distance R_e. The pixel area A_e is constant and is not a function of the radial location. Note that prefactor 1/2 appears in the expression due to axisymmetry and R_e = number of pixels along the radial axis between i^{th} pixel and axisymmetric axis $\times$ size of a pixel.

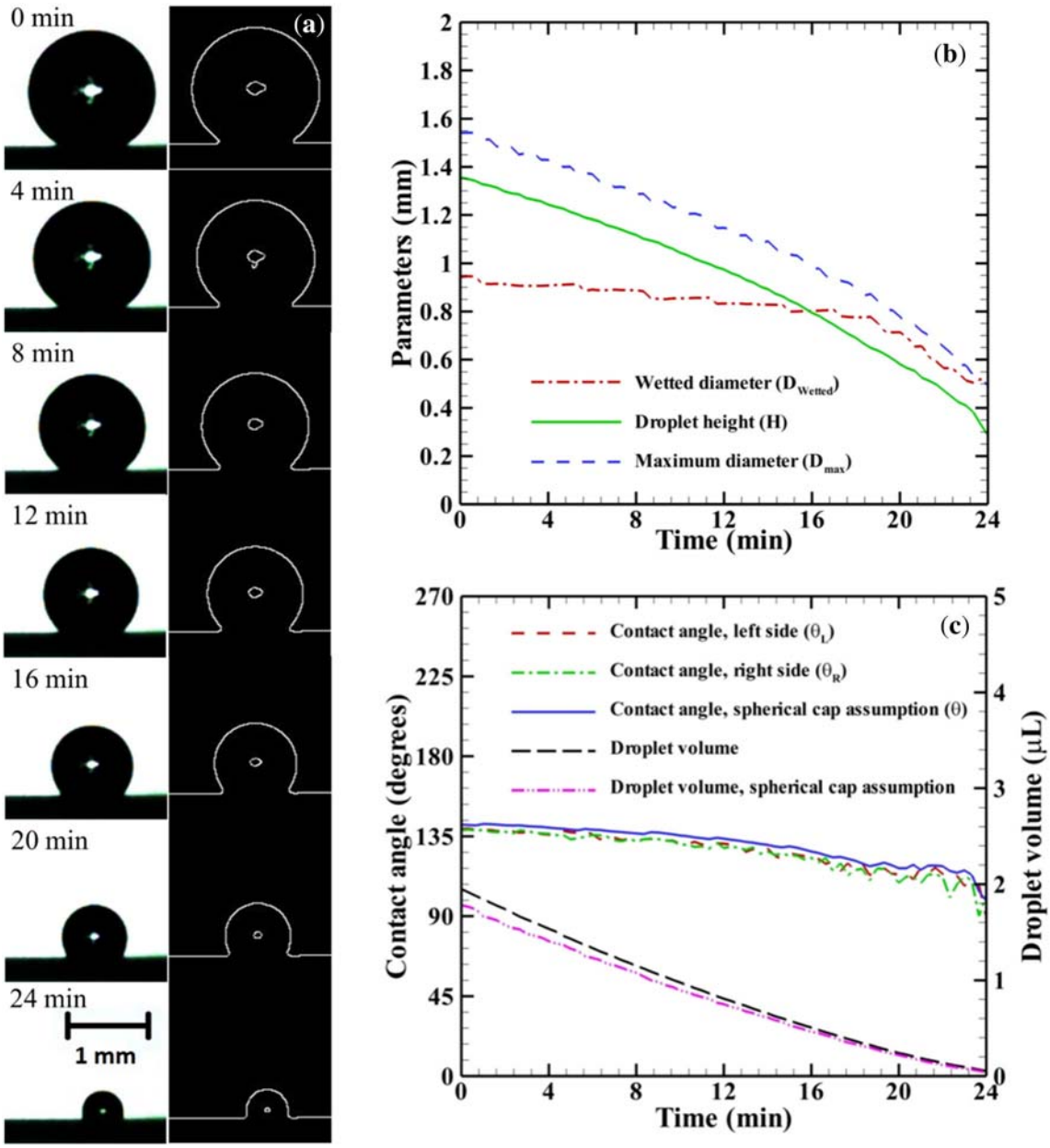

Figure 6. (a) Time-variation of recorded shapes of the water droplet during evaporation on a hydrophobic surface (left column) and measured droplet shapes using the present method (right column), (b) Measured droplet dimensions using the present method, (c) Measured dynamic contact angle and droplet volume. The measured droplet volume is compared with the theoretical value with the assumption of droplet shape as a spherical cap.

3. Results and discussion

We present three case studies to test the proposed method, namely, sessile droplet evaporation on a hydrophobic surface, bouncing droplet on a hydrophobic surface, and viscous droplet spreading on a surface. The high-speed visualization videos from the experiments served as test cases for the proposed image processing method in section 2.

3.1 *Evaporating droplet on a hydrophobic surface*

We recorded the evaporation of a water droplet gently deposited onto a hydrophobic surface with 5 frames per second. The ambient temperature and relative humidity are 27.1°C and 37%, respectively. The time-varying droplet shapes obtained by the high-speed camera are plotted in the left column of figure 6a. We plot the corresponding processed images with the liquid-gas interface and liquid-solid interface obtained using the proposed method in the right column of figure 6a. The

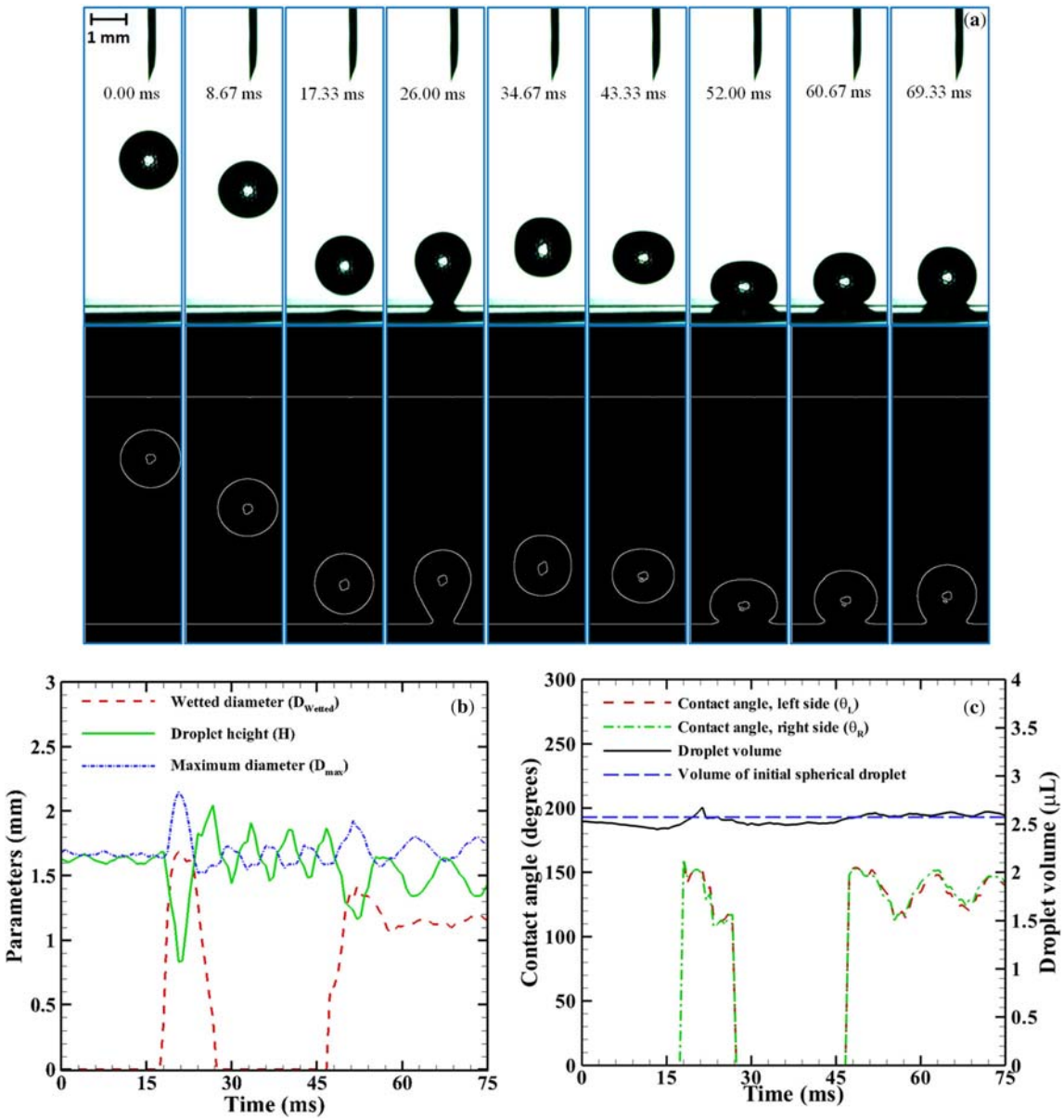

Figure 7. (a) Time-varying droplet shapes for bouncing water droplet obtained from high-speed visualization (top row) and those obtained using the proposed method (bottom row), (b) Time-varying droplet wetted diameter, maximum diameter and height are plotted during bouncing and second impact, (c) Measured dynamic contact angle and droplet volume as a function of time. The measured volume is compared with the theoretical value.

number of pixels across the droplet height varies from 92 (0 min) to 24 (24 min) pixels in figure 6(a). The time variation of the wetted diameter, maximum diameter, and height are plotted in figure 6b.

In figure 6c, we present the profile of the dynamic contact angle for the left as well as right side and droplet volume. The verification of the measured values was performed by available theoretical expressions. Since the droplet size is lesser than the capillary length ($\sim$2.7 mm for water), the theoretical expressions of the contact angle and volume are $\tan(\theta/2) = h/r$ and $V = \pi h(3r^2+h^2)/6$, assuming the sessile droplet as a spherical cap, where h and r are the droplet height and wetted radius, respectively. In figure 6c, the mean difference between the measured left side contact angle and the theoretical value is 3.64° with a standard deviation of 1.68°. Similarly, for the right side contact angle, the mean difference and standard deviation are 4.65° and 2.22°, respectively. The measured volume is 10.14% of the theoretical volume (figure 6c).

The oscillations in the dynamic contact angle at the end of the evaporation can be attributed to the fact that there are very few pixels left for the fitting of the polynomial and the method does not work well in this situation. Nonetheless, the proposed method captures correctly the evolution of the contact angle for around 85% of the total evaporation time. The measured evaporation rate of the water droplet in figure 6c is around

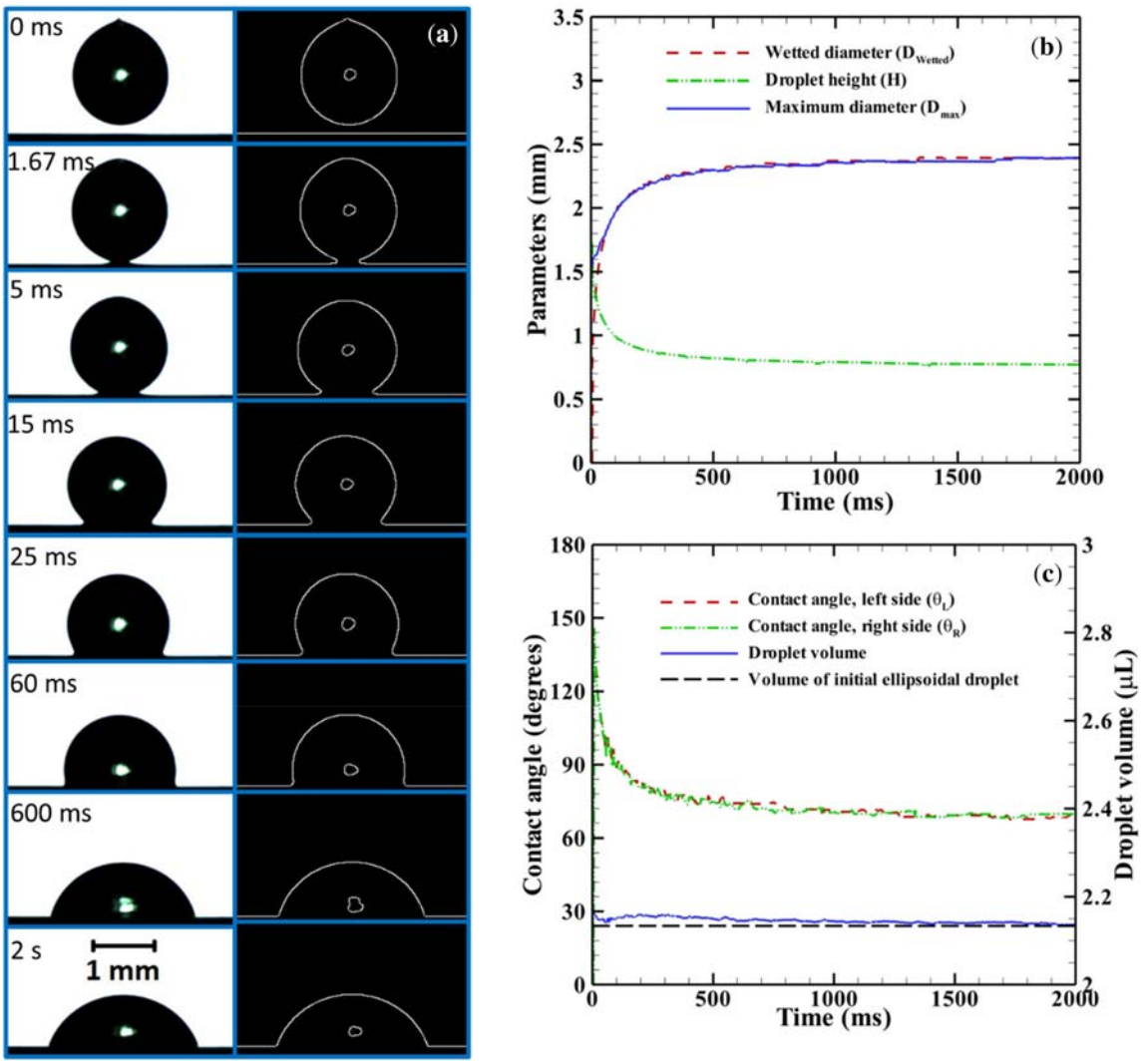

Figure 8. (a) Time-varying shapes for the viscous spreading of glycerol droplet obtained from high-speed visualization (left column) and those obtained using the proposed method (left column), (b) Droplet diameter and height is plotted as a function of time, (c) Time-variation of the droplet volume and dynamic contact angles on left and right side of the axis of symmetry. The constant theoretical volume is also plotted for the comparison with the measured volume.

1.4×10^{-12} kg/s, assuming a linear decay of the volume with time.

3.2 *Bouncing droplet on a hydrophobic surface*

Figure 7a plots the droplet shapes recorded at 1500 frames per second using a high-speed camera during the impact of a water droplet on a hydrophobic surface with an impact velocity of 0.3431 m/s just before the impact. The experiment was carried out with the ambient temperature as 25.4°C and humidity of 37%. The droplet completely bounces and impacts again on the solid surface, as shown in figure 7a, top row. The proposed method successfully captures the complex topology of the liquid-gas interface during bouncing and further impact on the substrate, as plotted in figure 7a, bottom row. In figure 7b, we present the time-variation of droplet dimensions - droplet height, maximum diameter, wetted diameter. Note that wetted diameter is zero while the droplet is in air and using the proposed method, contact line velocity can easily be plotted as time-derivative of the droplet wetted diameter.

In figure 7c, we present the profiles of the dynamic contact angle as well as droplet volume. Since the evaporation time of the droplet is around four orders of magnitude larger than the bouncing time (see section 3.2 in Ref. [7] for justification), the evaporation is negligible and the measured droplet volume is almost constant, as plotted in figure 7c. We compare the measured droplet volume with the initial droplet theoretical volume (before impact), assuming the droplet as sphere. The measured volume is within 7.7% of the theoretical volume. The maximum error in the volume measurement with respect to theoretical volume is around 4% and the error at $t = 0$ ms is around 2%. The minor change in the error with time could be attributed to the fact that droplet loses sphericity as it travels in air, which can be confirmed by comparing images from 0 to 17.33 ms in figure 7(a). Further, the impact may not be perfectly axisymmetric and the algorithm for volume measurement described in section 2.4 assumes an axisymmetric geometry of the droplet. This factors could induce minor errors in the volume measurement.

3.3 *Viscous droplet spreading*

Finally, we record the spreading of a glycerol droplet on a silicon wafer with an impact velocity of 0.19 m/s at 3000 frames per second with the ambient temperature of 26.6°C and relative humidity of 37%. We plot the viscous droplet spreading and corresponding liquid-gas interface obtained from the proposed method in figure 8a. The time-variation of the droplet dimensions and contact angle are presented in figure 8b and figure 8c, respectively. In figure 8c, the measured volume is compared with the respective theoretical value. The latter is calculated for an axisymmetric ellipsoidal shape, as noted in figure 8a, $t = 0$ ms. The theoretical droplet volume is given by, $V = \pi h d^2/6$, where h is the height of the droplet along the axis of symmetry and d is the diameter of the droplet normal to the axis of symmetry. The measured volume is within 0.55% of the theoretical value, demonstrating the accuracy of the proposed method.

4. Conclusions

We have demonstrated high-speed visualization and an associated image processing based method for the measurements of time-varying droplet dimensions, contact angle, and volume during the droplet impact and evaporation on a solid surface. The microliter droplets are generated using a syringe at ambient temperature and the droplet shapes are recorded using a high-speed camera. The image processing method is based on edge detection using Canny's method with a threshold obtained by the Otsu method. A higher-order polynomial is fitted along the pixels near the contact line to measure the dynamic contact angle. We estimate around 3% error in the measured contact angle as compared to the known analytical value for a second-order polynomial fitted on 15 pixels near the contact line. The time-varying droplet dimensions, namely, wetted diameter, maximum diameter, height, are plotted by fitting a sigmoid function for pixel intensity across the liquid-gas interface. Our method calculates the droplet volume by identifying the pixels inside the droplet and numerically integrating them in axisymmetric coordinates.

We test the method for three different cases of the droplet interaction with a solid surface, namely, sessile droplet evaporation on a hydrophobic surface, bouncing droplet on a hydrophobic surface, and viscous droplet spreading on a surface. The measurements using the proposed method are compared with the theoretical values, wherever possible. The sources of the possible errors are identified and are briefly explained. Overall, the comparisons between the measurements obtained by the proposed method and the respective values obtained by the available analytical theories are in good agreement and verify the fidelity of our method. The proposed method can also be easily extended to calculate the impact velocity while the droplet is in air and contact line velocity during spreading, by numerically integrating the time-variation of droplet height and wetted radius, respectively.

Acknowledgements

We gratefully acknowledge financial support by a grant (EMR/2016/006326) from the Science and Engineering Research Board (SERB), Department of Science and Technology (DST), New Delhi, India.

References

[1] Patil N D and Bhardwaj R 2014 Evaporation of a microdroplet on a hydrophobic substrate. *Int. J. Micro-Nano Scale Transport* 5: 51–58

[2] Attinger D, Frankiewicz C, Betz A R, Schutzius T M, Ganguly R, Das A, Kim C-J and Megaridis C M 2014 Surface engineering for phase change heat transfer: a review. *MRS Energy Sustain. Rev. J.* 1: E4

[3] Patil N D and Bhardwaj R 2019 Recent developments on colloidal deposits obtained by evaporation of sessile droplets on a solid surface. *J. Indian Inst. Sci.* 99: 143–156

[4] Chatterjee S, Kumar M, Murallidharan J S and Bhardwaj R 2020 Evaporation of initially heated sessile droplets and the resultant dried colloidal deposits on substrates held at ambient temperature. *Langmuir* 36: 8407–8421

[5] Bhardwaj R, Longtin J P and Attinger D 2010 Interfacial temperature measurements, high-speed visualization and finite-element simulations of droplet impact and evaporation on a solid surface. *Int. J. Heat and Mass Transfer* 53: 3733–3744

[6] Kumar M and Bhardwaj R 2020 Wetting characteristics of Colocasia esculenta (Taro) leaf and a bioinspired surface thereof. *Sci. Rep.* 10: 1–15

[7] Bhardwaj R and Attinger D 2008 Non-isothermal wetting during impact of millimeter-size water drop on a flat substrate: numerical investigation and comparison with high-speed visualization experiments. *Int. J. Heat Fluid Flow* 29: 1422–1435

[8] Huhtamäki T, Tian X, Korhonen J T and Ras R H 2018 Surface-wetting characterization using contact-angle measurements. *Nat. Prot.* 13: 1521–1538

[9] Chini S F and Amirfazli A 2011 A method for measuring contact angle of asymmetric and symmetric drops. *Colloids Surfaces A Physicochem. Eng. Aspects* 388: 29–37

[10] Rotenberg Y, Boruvka L and Neumann A W 1983 Determination of surface tension and contact angle from the shapes of axisymmetric fluid interfaces. *J. Colloid Interface Sci.* 93: 169–183

[11] Skinner F K, Rotenberg Y and Neumann A W 1989 Contact angle measurements from the contact diameter of sessile drops by means of a modified axisymmetric drop shape analysis. *J. Colloid Interface Sci.* 130: 25–34

[12] Hoorfar M and Neumann A W 2006 Recent progress in axisymmetric drop shape analysis (ADSA) *Adv. Colloid Interface Sci.* 121: 25–49

[13] Tavana H and Neumann A W 2007 Recent progress in the determination of solid surface tensions from contact angles. *Adv. Colloid Interface Sci.* 132: 1–32

[14] Kalantarian A, David R and Neumann A W 2009 Methodology for high accuracy contact angle measurement. *Langmuir* 25: 14146–14154

[15] Bateni A, Susnar S S, Amirfazli A and Neumann A W 2003 A high-accuracy polynomial fitting approach to determine contact angles. *Colloids Surfaces A Physicochemi. Eng. Aspects* 219: 215–231

[16] Stalder A F, Kulik G, Sage D, Barbieri L and Hoffmann P 2006 A snake-based approach to accurate determination of both contact points and contact angles. *Colloids Surfaces A Physicochem. Eng. Aspects* 286: 92–103

[17] Thurow K, Krüger T and Stoll N 2009 An optical approach for the determination of droplet volumes in nanodispensing, *J. Automated Methods Manag. Chem.* 2009: 198732

[18] Arcamone J, Dujardin E, Rius G, Perez-Murano F and Ondarcuhu T 2007 Evaporation of femtoliter sessile droplets monitored with nanomechanical mass sensors. *J. Phys. Chem. B* 111: 13020–13027

[19] Patil N D, Bhardwaj R and Sharma A 2016 Droplet impact dynamics on micropillared hydrophobic surfaces. *Exp. Therm. Fluid Sci.* 74: 195–206

[20] http://www.virtualdub.org

[21] http://www.mathworks.com

[22] Canny J 1986 A computational approach to edge detection. *IEEE Trans. Pattern Anal. Mach. Intell.* 8: 679–698

[23] Canny's method is implemented as a function named 'edge' in Matlab® 2014. Details are given at www.mathworks.com/help/images/ref/edge.html

[24] Otsu N 1979 A threshold selection method from gray-level histograms. *IEEE Trans. Syst. Man Cyber.* 9: 62–66

[25] Otsu's method is implemented as a function named 'graythresh' in Matlab® 2014. Details are given at www.mathworks.com/help/images/ref/graythresh.html

[26] The method computes the perimeter by calculating the distance between each adjoining pair of pixels in the liquid-gas interface. It is implemented as a function named 'bwpropfilt' in Matlab® 2014. Details are given at www.mathworks.com/help/images/ref/bwpropfilt.html

[27] Soille P 1999 *Morphological Image Analysis: Principles and Applications.* Springer-Verlag, Berlin Heidelberg, pp 173–174

[28] This algorithm is implemented as a function named 'imfill' in Matlab® 2014. Details are given at www.mathworks.com/help/images/ref/imfill.html